Time-resolved resonance Raman and density functional theory study of the photochemistry of 4-benzoylpyridine in acetonitrile and 2-propanol

ARTICLE *in* JOURNAL OF RAMAN SPECTROSCOPY · APRIL 2008

Impact Factor: 2.67 · DOI: 10.1002/jrs.1869

5 AUTHORS, INCLUDING:

Yong Du
China Jiliang University
46 PUBLICATIONS **422** CITATIONS
SEE PROFILE

Chensheng Ma
The University of Hong Kong
82 PUBLICATIONS **1,807** CITATIONS
SEE PROFILE

Wai-Ming Kwok
The Hong Kong Polytechnic University
141 PUBLICATIONS **4,005** CITATIONS
SEE PROFILE

David Lee Phillips
The University of Hong Kong
345 PUBLICATIONS **7,041** CITATIONS
SEE PROFILE

JOURNAL OF RAMAN SPECTROSCOPY
J. Raman Spectrosc. 2008; **39**: 503–514
Published online 5 February 2008 in Wiley InterScience
(www.interscience.wiley.com) DOI: 10.1002/jrs.1869

JRS

Time-resolved resonance Raman and density functional theory study of the photochemistry of 4-benzoylpyridine in acetonitrile and 2-propanol

Yong Du, Jiadan Xue, Chensheng Ma, Wai Ming Kwok and David Lee Phillips*

Department of Chemistry, The University of Hong Kong, Pokfulam Road, Hong Kong, P. R. China

Received 4 September 2007; Accepted 10 October 2007

A nanosecond time-resolved resonance Raman (ns-TR^3) spectroscopic investigation of the intermolecular hydrogen-abstraction reaction of the triplet state of 4-benzoylpyridine (4-BPy) in 2-propanol solvent is reported. The TR^3 results reveal a rapid hydrogen abstraction (<10 ns) by the 4-BPy triplet state ($n\pi^*$) with the 2-propanol solvent, leading to formation of a 4-BPy ketyl radical and an associated dimethyl ketyl radical partner from the solvent. The recombination of these two radical species occurs with a time constant about 200 ns to produce a *para*-N-LAT (light absorbing transient). The structure, major spectral features, and identification of the ketyl radical and the *para*-N-LAT coupling complex have been determined and confirmed by comparison of the TR^3 results with results from density functional theory (DFT) calculations. A reaction pathway for the photolysis of 4-BPy in 2-propanol deduced from the TR^3 results is also presented. The electron-withdrawing effect of the heterocyclic nitrogen for 4-BPy on the triplet state makes it have a significantly higher chemical reactivity for the hydrogen abstraction with 2-propanol compared to the previously reported corresponding benzophenone triplet reaction under similar reaction conditions. In addition, the 4-BPy ketyl radical reacts with the dimethyl ketyl radical to attach at the *para*-N atom position of the pyridine ring to form a cross-coupling product such as 2-[4-(hydroxy-phenyl-methylene)-4h-pyridin-1-yl]-propan-2-ol instead of attacking at the *para*-C atom position as was observed for the corresponding benzophenone reaction reported in an earlier study. Copyright © 2008 John Wiley & Sons, Ltd.

Supplementary electronic material for this paper is available in Wiley InterScience at http://www.interscience.wiley.com/jpages/0377-0486/suppmat/

KEYWORDS: 4-benzoylpyridine; hydrogen abstraction; ketyl radical; resonance Raman spectroscopy; time-resolved spectroscopy

INTRODUCTION

The photochemistry and photophysics of benzophenone (BP) and its derivatives have been the subjects of many studies owing to their importance for understanding the mechanisms of electron transfer and hydrogen abstraction in electronic excited states.[1–55] Most of these studies have been done to elucidate the mechanism of photoreduction reactions undergone by the aromatic carbonyl compounds in the presence of a hydrogen atom donor.[1,2,8,28–41] Although the basic mechanism for the photoreduction of BP was deduced more than 40 years ago by Moore *et al.*,[2] there has been a sustained interest in elucidating more details and better characterization of this fundamental reaction as advances in technology and spectroscopic methods have become available.[3–46,55] The lowest excited singlet (S_1 $n\pi^*$) and triplet (T_2 $\pi\pi^*$) states typically exhibit a small energy gap and are strongly coupled via a spin–orbit interaction[23,24] that enables intersystem crossing (ISC) to kinetically compete very well with other S_1 state processes such as internal conversion (IC) and fluorescence emission. Therefore, the T_1 state is formed with a yield close to unity in most cases.[1–24] In most systems, the major relaxation pathway of photoexcited BP molecule to the ground state occurs via the T_1 state, which is also usually responsible for all of the major photochemical reactions of BP and its derivatives in the solution phase.

The T_1 state of BP has $n\pi^*$ character with the excitation localized on the carbonyl group in many types of solvents.[1–24,42–45] Hamaguchi and coworkers[42–45] observed the transient resonance Raman spectra of the T_1 state of BP and confirmed that the $n\pi^*$ triplet state is efficiently

*Correspondence to: David Lee Phillips, Department of Chemistry, The University of Hong Kong, Pokfulam Road, Hong Kong, P. R. China. E-mail: phillips@hkucc.hku.hk

photoreduced by hydrogen atom donors with the photolysis of BP in H-donor organic solvents such as isopropyl alcohol (also known as 2-propanol) leading to hydrogen abstraction from the solvent by the ketone to form a diphenylketyl (DPK) radical,[42–45] consistent with a number of past photochemical investigations.[1–24] The DPK radical and the species produced from the H-donor solvent react to produce an intermediate(s) called 'light absorbing transient' (LATs), which has been examined by a variety of experimental methods such as transient absorption spectroscopy.[28–41] Time-resolved resonance Raman (TR^3) spectroscopy was recently used to characterize the T_1 state of BP, the DPK radical and the long-lived LAT intermediate that was assigned explicitly to a 2-[4-(hydroxyl-phenyl-methylene)-cyclohexa-2,5-dienyl]-propan-2-ol cross-coupling product (referred to hereafter as the *para*-DPK-dimethylketyl (DMK) species in this paper) formed from the cross-coupling reaction of the DPK radical and the DMK radical.[55]

The substituents on the aromatic rings of BP derivatives influence the relative energies of the two types of electronic excited states ($n\pi^*$ and $\pi\pi^*$ states) in both the singlet and triplet manifolds.[47–54] The reactivity of these substituted BP derivatives varies widely with the nature of the substituent and solvent.[47–54] The electron-withdrawing effect of the heterocyclic nitrogen enhances the $n\pi^*$ character of the triplet and this increases the substituted BPs ability for abstracting hydrogen from 2-propanol (the molecular structures of BP and 4-benzoylpyridine (4-BPy) are shown in Scheme 1). This hydrogen-abstraction reaction has a high quantum yield for producing the ketyl radical intermediate via the $n\pi^*$ triplet excited state reaction with the hydrogen donor after laser flash photolysis (LFP) of the substituted BP in room temperature solutions. These aspects have been widely studied by various experimental methods, including transient absorption spectroscopy.[47–54,56]

In the present work, TR^3 experiments were performed on 4-BPy in acetonitrile (MeCN) and 2-propanol solvents in order to examine the electron-withdrawing effect of the heterocyclic nitrogen on the triplet state structure and property as well as its effect on the photoreduction species produced subsequent to the hydrogen-abstraction reaction with 2-propanol. The TR^3 spectra were obtained with two different probe excitation wavelengths in 2-propanol solvent so as to characterize the 4-BPy ketyl radical and the long-lived LAT intermediate for this system which was assigned to the coupling complex from the 4-BPy ketyl radical reacting with the partner DMK radical formed from the hydrogen donor 2-propanol molecule. To our knowledge, this is the first TR^3 characterization of these intermediates and dynamics for photoreduction of 4-BPy in 2-propanol. To help determine the intermediate species geometries and vibrational wavenumbers, and to make assignments of the experimental vibrational bands, density functional theory (DFT) calculations were done using the (U)B3LYP methods with a 6-311G** basis set for all of the species examined here. The structure and properties of the 4-BPy triplet excited state, 4-BPy ketyl radical, and *para*-4-BPy-DMK intermediate are also briefly discussed. The results for 4-BPy in 2-propanol here are compared to those for the analogous BP reactions in 2-propanol to reveal the electron-withdrawing effect of the heterocyclic nitrogen on the structures, properties, and chemical reactivity of the reaction intermediates observed in both systems.

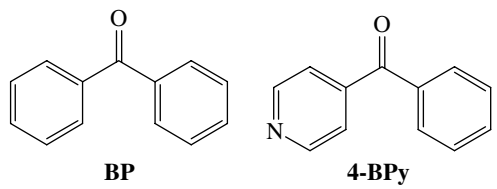

Scheme 1. Molecular structures of benzophenone (BP) and 4-benzoylpyridine (4-BPy).

EXPERIMENTAL AND COMPUTATIONAL METHODS

The 4-BPy sample was commercially obtained from Aldirich (with >99% purity) and used as received. Spectroscopic grade MeCN, 2-propanol, and deionized water were used as solvents for the experiments presented in this work. Sample solutions of ~3 mM concentration were employed in the TR^3 experiments.

The ns-TR^3 measurements were done using an experimental apparatus described previously.[57–63] The pump wavelength was 266 nm supplied by the fourth harmonic of a neodymium–doped yttrium aluminium garnet (Nd : YAG) Q-switched laser. The 319.9 nm probe wavelength came from the third anti-Stokes of a hydrogen Raman-shifted line pumped by the second harmonic (532 nm), and the 354.7 nm probe wavelength came from the third harmonic from the second Nd : YAG laser (Spectra Physics GCR-150-10). The time delay between the pump and probe beam was controlled electronically by a pulse delay generator and was monitored by a photodiode and a 500 MHz oscilloscope; the time resolution of the experiments was estimated to be ~5–10 ns. The energy of the pump and the probe pulses was in the 2.5–3.5 mJ range with a repetition rate of 10 Hz, and a near-collinear geometry was used to focus the pump and probe beam onto a flowing liquid stream of the sample. The Raman scattering was collected in a backscattering configuration and detected by a liquid-nitrogen-cooled charge-coupled device (CCD) detector where the measurements were performed under open air and under oxygen being bubbled through the sample solution. The Raman signal was acquired by the CCD for 30–60 s before being read out to an interfaced PC and about 10–20 of these readouts were added together to obtain a resonance Raman spectrum. The spectra presented in this work were obtained from subtraction of an appropriately scaled probe-before-pump

DOI: 10.1002/jrs

spectrum from the corresponding pump–probe spectrum, and MeCN Raman bands were used to calibrate the TR^3 spectra with an estimated accuracy of $\pm 5\ cm^{-1}$ in absolute wavenumber. A Lorentzian function was used to determine the areas of the relevant Raman bands in the TR^3 spectra and to extract the decay and growth of the species seen in the experiments.

The optimized geometry, vibrational modes, and vibrational wavenumbers for the ground-state 4-BPy, the triplet-state 4-BPy, the 4-BPy ketyl radical, as well as the 4-BPy coupling complex were obtained from (U)B3LYP DFT calculations using a 6-311G** basis set and no imaginary wavenumber modes were observed at any of the optimized structures shown here. A Lorentzian function with a 15 cm^{-1} bandwidth was used in conjunction with the calculated Raman vibrational wavenumbers and relative intensities to determine the (U)B3LYP/6-311G** calculated Raman spectra presented here. Time dependent-density functional theory (TD-DFT) calculations were performed for the species of interest to estimate the electronic transition energies and their oscillator strengths. The values obtained were compared with the TR^3 results and literature transient absorption experimental results where available. All calculations were performed with Gaussian 03 programs.[64,65]

RESULTS AND DISCUSSION

Steady state photolysis of 4-BPy in 2-propanol

The ground-state absorption spectra of 4-BPy in MeCN and 2-propanol with the pump and probe wavelengths used in the TR^3 measurements (indicated by arrows above the spectra) are shown in Fig. 1. Figure 2 displays the spectral changes observed following the irradiation of ~0.08 mM 4-BPy in 2-propanol. The decrease of the intense $\pi\pi^*$ band of the ketone with a maximum at 263 nm is accompanied

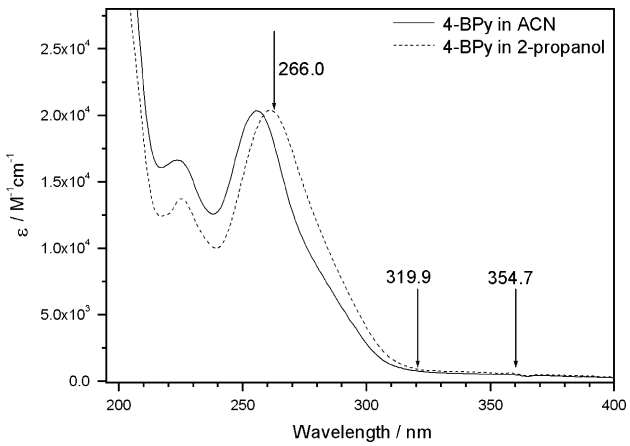

Figure 1. Absorption spectra of 4-BPy in acetonitrile (solid line) and 2-propanol (dotted line). The 266 nm pump and 319.9, 354.7 nm probe wavelengths used in the TR^3 measurements are indicated by the arrows above the spectra.

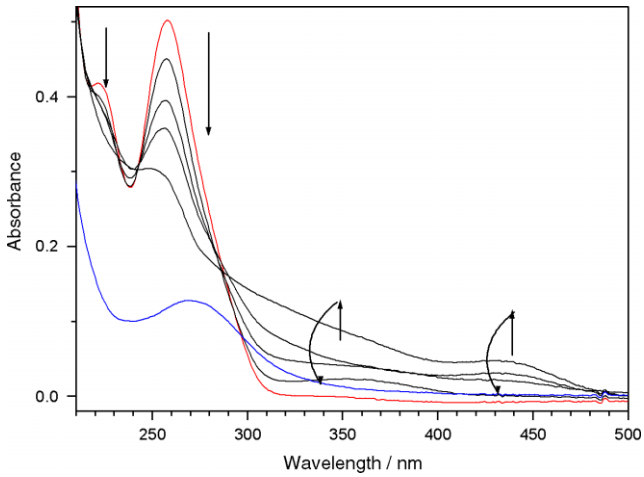

Figure 2. Absorption spectra observed following varying irradiation times using 266 nm light of 0.08 mM 4-BPy in 2-propanol. The cell path length is 10 mm. Irradiation times: 0 s (red line), 10, 20, 30, 50, and 600 s (blue line). Incident photons $2 \times 10^{15}\ s^{-1}$. This figure is available in colour online at www.interscience.wiley.com/journal/jrs.

by an increase of the absorption in the 300–450 nm region, which has a maximum at 435 nm and a shoulder around 360 nm. With longer irradiation times (e.g. about 600 s), the absorption bands in the 300–450 nm region completely disappear and a new band located at 270 nm is observed.

The most likely candidates for the photoproduct in the first several 10 s in Fig. 2 is the so-called LAT, which can be tentatively assigned to the coupling of the 4-BPy ketyl radical and the dimethyl ketyl radical from 2-propanol molecule on the basis of the analogous photochemistry of BP in 2-propanol.[55] This structure was demonstrated to be mostly easily formed when the ketyl radicals are produced from the BP in the same solvent. In the subsequent sections of this paper, ns-TR^3 spectroscopy with two probe wavelengths (319.9 and 354.7 nm) was performed to characterize the properties of the 4-BPy ketyl radical and the LAT formed from the coupling of the two radicals. Combined with results from DFT calculations, the structures and the vibrational assignment of these intermediates are also discussed and compared to similar results previously reported for the photolysis of BP in 2-propanol.[55]

Time-resolved resonance Raman spectra of 4-BPy in MeCN: the triplet state of 4-BPy

Figure 3 shows the ns-TR^3 spectra of 4-BPy in pure MeCN obtained under open air (a) and oxygen purge (b) conditions at various time delays from 0 ns to 1.5 μs using a 266 nm pump wavelength and a 319.9 nm probe wavelength. The 266 nm pump wavelength excites the strong $\pi-\pi^*$ transition of 4-BPy. The time dependence of the 975 cm^{-1} band area of the intermediate after photolysis 4-BPy in MeCN observed in Fig. 2 are shown along with an exponential fitting of the data that was used to follow the kinetics of this species

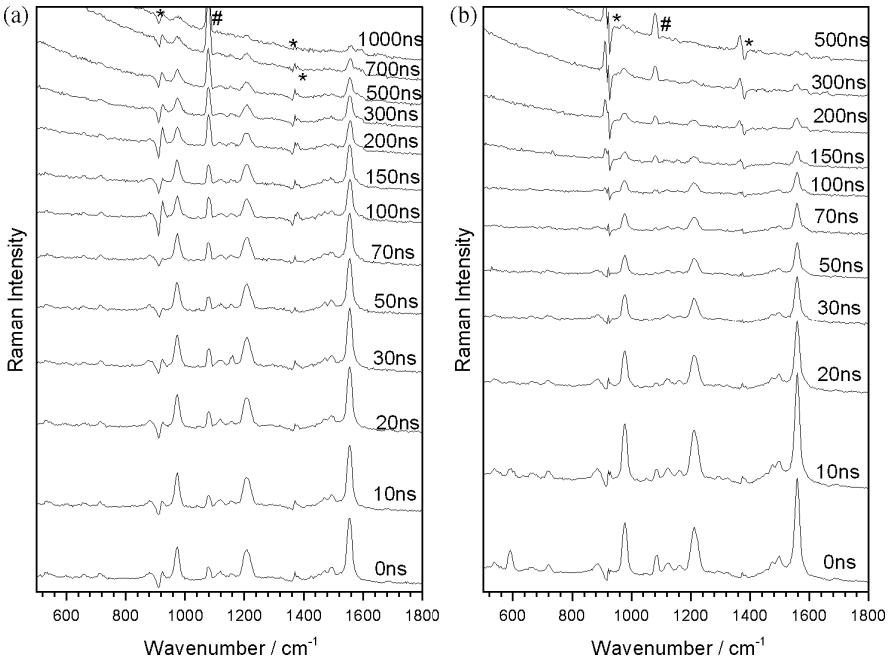

Figure 3. Nanosecond time-resolved resonance Raman spectra of 4-BPy in pure acetonitrile obtained under open air (a) and O_2 purge (b) with 266.0 nm pump excitation wavelength and 319.9 nm probe wavelength at various delay times that indicated next to the spectra. The asterisk (*) marks solvent subtraction artifacts and the # band is due to stray laser line.

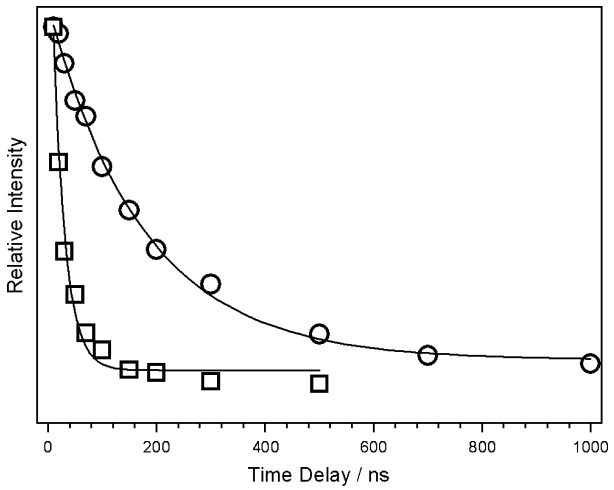

Figure 4. Time dependence of the 975 cm^{-1} band area obtained in Fig. 3.

at 1209 cm^{-1} Raman band under open air (open circles) and O_2 purge (open squares) conditions. The kinetics in Fig. 4 for this 4-BPy intermediate can be fitted very well by an one exponential decay function with time constants of about 176 ± 9 ns for open air and 23 ± 2 ns under O_2 purge conditions. The significant decrease of the lifetime of the intermediate under O_2 purge conditions indicates that the 4-BPy intermediate observed is likely triplet in nature.

To verify the triplet state 4-BPy assignment for the intermediate observed in the TR^3 spectra of Fig. 3, DFT calculations were done and these results were compared with the experimental spectra. Figure 5 displays a comparison between the experimental TR^3 spectrum obtained at 10 ns in Fig. 3(a) and the UB3LYP/6-311G** DFT-calculated normal Raman spectrum of the triplet state 4-BPy. Preliminary Raman band assignments for the 4-BPy triplet state were made on the basis of the correlation between the experimental and calculated Raman spectra shown in Fig. 4. Table 1S (see Supplementary Material) lists these tentative vibrational assignments along with the nominal descriptions of the normal modes. Six major Raman bands, at 975, 1121, 1209, 1499, 1569, and 1590 cm^{-1}, were observed. Most of the Raman bands seen in the TR^3 spectra of the 4-BPy triplet state are due to vibrations associated with the ring C–C stretch and C–H bend motions. The 1590 and 1569 cm^{-1} Raman bands are mainly due to a ring C–C and C–N stretch vibrational mode. The 1499 cm^{-1} Raman band is associated with a C–H in-plane bending of the ring vibrational motion. The 1209 cm^{-1} Raman band is mostly from a T_1 carbonyl C–O stretching mode which is substantially downshifted compared to the ground-state 4-BPy carbonyl stretch band, similar to results for the triplet BP. The 1121 cm^{-1} Raman band is due to a combination of the C–H in-plane bending of the ring vibrational motion and C3–C1–C9 bending. The 975 cm^{-1} Raman band is attributed to the C–C–C and C–N–C bending or the so-called *ring deformation mode*. Figure 5 reveals that the calculated Raman spectrum shows reasonable agreement with the experimental TR^3 spectrum for the 4-BPy triplet state in terms of the vibrational wavenumbers. However, a close

DOI: 10.1002/jrs

examination shows differences between the relative intensity patterns of the experimental spectrum and the calculated spectrum in Fig. 5. This can be attributed to the experimental spectrum being resonantly enhanced while the calculated spectrum is a nonresonant Raman spectrum.

Figure 6 shows a simple diagram of the optimized geometry and selected structural parameters obtained from (U)B3LYP/6–311G** calculations for the 4-BPy ground and triplet states. Computed structural parameters for the 4-BPy ground and triplet state are listed in Table 1. The bond lengths vary substantially on going from the ground state to the triplet state. Comparison of the triplet state structure with that for the ground state reveals that the carbonyl bond is lengthened by about 0.1 Å while the C1–C3 and C1–C9 bonds which connect the carbonyl group and the two phenyl rings are shortened by about 0.071 and 0.040 Å to become about 1.436 and 1.457 Å, respectively, in the triplet state (Fig. 6 and Table 1). The wavenumber of the carbonyl C–O stretch dominated mode is characteristic in reflecting the nature and properties of the triplet states for aromatic carbonyl compounds. For the 4-BPy triplet state, the remarkable downshift of the triplet carbonyl stretch mode indicates that there is a strong weakening of this bond in the triplet state, and this is in agreement with the calculated 0.1 Å increase of the C–O bond length on going from the ground state to the triplet state. This also implies that the carbonyl group in the triplet state has a single-bond character as compared with the typical double C═O bond in the ground state.

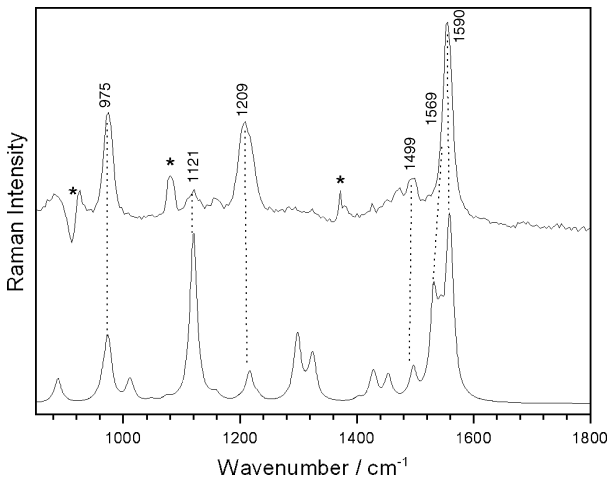

Figure 5. Comparison the experimental resonance Raman spectra of 4-BPy obtained in pure acetonitrile 10 ns delay time (top) and with the DFT-calculated spectra for the triplet 4-BPy (bottom). The asterisk (*) marks solvent subtraction artifacts and the # band is due to stray laser line. Dotted lines display the correlation between the experimental and calculated Raman bands (see text for more details).

The electron-withdrawing effect of the heterocyclic nitrogen in ring A leads to a shortened C–O bond length of both the ground (by about 0.002 Å) and the triplet state of 4-BPy (by about 0.005 Å) compared with those of the parent BP reported earlier.[55] For the triplet state of 4-BPy, the N6–C5 and N6–C7 bond lengths (about 1.340 Å) are much shorter than C6–C5 and C6–C7 bond lengths (about 1.400 Å) of the triplet BP. This structural difference is in good agreement with the experimental results involving the ring C–C stretch mode which is at 1590/1569 cm^{-1} for 4-BPy whereas it is only 1542 cm^{-1} for BP (there is an upshift of 25 cm^{-1} or more from 4-BPy to BP due to the C–N bond length being shortened). From the computed total energy (including the zeropoint energy (ZPE)) for the 4-BPy triplet and the ground states, a triplet state energy of ~262.9 kJ mol^{-1} can be estimated. This value is smaller than the ~270.0 kJ mol^{-1} triplet energy analogous estimate for BP. This is consistent with the results that the hydrogen-abstraction reaction of 4-BPy in 2-propanol takes place more easily than that of BP as will be discussed in the next section.

Time-resolved resonance Raman spectra of 4-BPy in 2-propanol: the 4-BPy ketyl radical and *para*-N-LAT species

Figure 7 shows the ns-TR[3] spectra of 4-BPy in 2-propanol obtained at different time delays from 0 ns to 50 μs using a 266-nm pump wavelength and a 319.9-nm probe wavelength (a) and 354.7 nm probe wavelength (b). When these two probe wavelengths are used, the 4-BPy triplet state signal cannot be seen at early time delays in the 0–10 ns range,

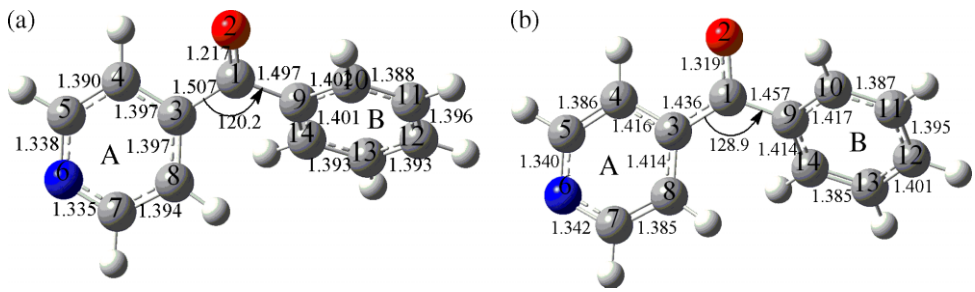

Figure 6. Optimized structure of the ground state (a) and triplet state (b) of 4-BPy calculated from the B3LYP/6–31G** DFT calculations. Selected bond lengths (in Å) and bond angles (in deg) are labeled. This figure is available in colour online at www.interscience.wiley.com/journal/jrs.

DOI: 10.1002/jrs

Table 1. Structural parameters for the ground and triplet state of 4-BPy calculated from the DFT calculations using the (U)B3LYP methods and a 6-311G** basis set

Bond lengths (Å)			Bond angles(deg)			Dihedral angles(deg)		
	BPy(S_0)	BPy(T_0)		BPy(S_0)	BPy(T_0)		BPy(S_0)	BPy(T_0)
C1–O2	1.217	1.319	C1–C3–C4	118.6	120.6	C1–C3–C4–C5	−177.2	−178.4
C1–C3	1.507	1.436	C1–C9–C10	117.8	119.4	C1–C9–C10–C11	−177.8	−178.5
C1–C9	1.497	1.457	C3–C1–O2	119.1	118.7	O2–C1–C3–C4	30.7	14.4
C3–C4	1.397	1.416	C3–C1–C9	120.2	128.9	O2–C1–C9–C10	23.8	31.7
C4–C5	1.39	1.386	C9–C1–O2	120.7	112.3	C3–C4–C5–N6	1.4	0.1
C5–N6	1.338	1.34	C3–C4–C5	118.9	119.2	C4–C5–N6–C7	−0.1	0.6
N6–C7	1.335	1.342	C4–C5–N6	123.7	124.4	C5–N6–C7–C8	−1.2	0
C7–C8	1.394	1.385	C5–N6–C7	117.1	116.3	N6–C7–C8–C3	0.9	−1.1
C8–C3	1.397	1.414	N6–C7–C8	123.8	124.6	C9–C10–C11–C12	1.3	0.3
C9–C10	1.402	1.417	C7–C8–C3	118.7	119	C10–C11–C12–C13	0	0.8
C10–C11	1.388	1.387	C8–C3–C4	117.8	116.5	C11–C12–C13–C14	−1	0.2
C11–C12	1.396	1.395	C9–C10–C11	120.4	120.4	C12–C13–C14–C9	0.7	−2.3
C12–C13	1.393	1.401	C10–C11–C12	120	120.4			
C13–C14	1.393	1.385	C11–C12–C13	120	119.7			
C14–C9	1.401	1.414	C12–C13–C14	120	120.7			
			C13–C14–C9	120.3	120.2			

while the BP triplet state signal could still be seen clearly under the same conditions.[55] This indicates that the 4-BPy triplet state probably has more $n\pi^*$ character than that of the BP triplet state. This could explain why the intermolecular hydrogen-abstraction reaction can take place more readily and efficiently to produce the 4-BPy ketyl radical compared to the BP ketyl radical. In the 0–20 μs time delay region and with a 319.9 nm probe wavelength used in the TR^3 experiments as shown in Fig. 7(a), one species is seen and is tentatively assigned to the 4-BPy ketyl radical on the basis of similar observations for the TR^3 spectra of several different ketyl radicals observed in our previous work[55] and those by Umapathy and coworkers.[66–69] From a comparison of the spectra in Fig. 7(a) obtained with a 319.9 nm probe wavelength with those in Fig. 7(b) obtained with a 354.7-nm probe wavelength, one can observe the same decay of the 4-BPy ketyl radical over the 0–10 μs time delay range at both wavelengths. There are some differences between the relative intensity patterns of the spectra, which can be attributed to the effect of using different probe wavelengths to acquire the 4-BPy ketyl radical resonance Raman spectra.

Strong signals are observed for the overtone and combination bands at 998, 1133, 1208, and 1593 cm^{-1} for the 319.9 nm probe wavelength TR^3 spectra (Fig. 10(b)). This implies that the 319.9 nm probe wavelength is significantly in resonance with a strong absorption band of the 4-BPy ketyl radical so that the vibrational bands of this species will be strongly resonantly enhanced in the TR^3 spectra acquired at that probe wavelength. This result is in very good agreement with previous LFP studies showing a characteristic strong 4-BPy ketyl radical absorption in the 320–340 nm region,[49] and this was also confirmed by results from TD-DFT calculations which found that the 4-BPy ketyl radical has one strong electronic transition at 317.4 nm with an oscillator strength of 0.315 (Table 4S). Assignments for the Raman bands observed in the TR^3 spectra for the 4-BPy ketyl radical were based on correlation to the Raman spectra predicted from the DFT calculations (Table 2S). Most of the fundamental Raman bands observed for the TR^3 spectra of the 4-BPy ketyl radical are due to vibrations associated with the ring C–C stretch and C–H bend motions. For example, the 998, 1133, and 1208 cm^{-1} vibrational bands have major contributions from ring C–H in-plane bend motions, whereas the 1575 and 1593 cm^{-1} vibrational bands have major contributions from the ring-center C–C stretch motions.

Examination of the TR^3 spectra in Fig. 7(a) reveals that the decay of the 4-BPy ketyl radical Raman signal is correlated with the growth of a new set of Raman features due to a new species. For the 319.9 nm probe wavelength TR^3 spectra (Fig. 7(a)), the intensity of the transient Raman signal for this new species is not very large. This suggests that the 319.9 nm probe wavelength is not fully resonant with the absorption band of this new species. To obtain stronger structural and kinetic information for this new species, additional TR^3 spectra were acquired using 354.7 nm probe wavelength and these spectra are displayed in Fig. 7(b). Examination of Fig. 7(b) shows that the 354.7 nm probe wavelength TR^3 spectra display a stronger TR^3 signal for the new species spectra relative to the 4-BPy ketyl radical spectra. This suggests the 354.7 nm probe wavelength is more in resonance with the absorption of the new species than the 319.9 nm probe wavelength used to obtain the TR^3 spectra in Fig. 7(a), and this new species has a characteristic 1661 cm^{-1} Raman

DOI: 10.1002/jrs

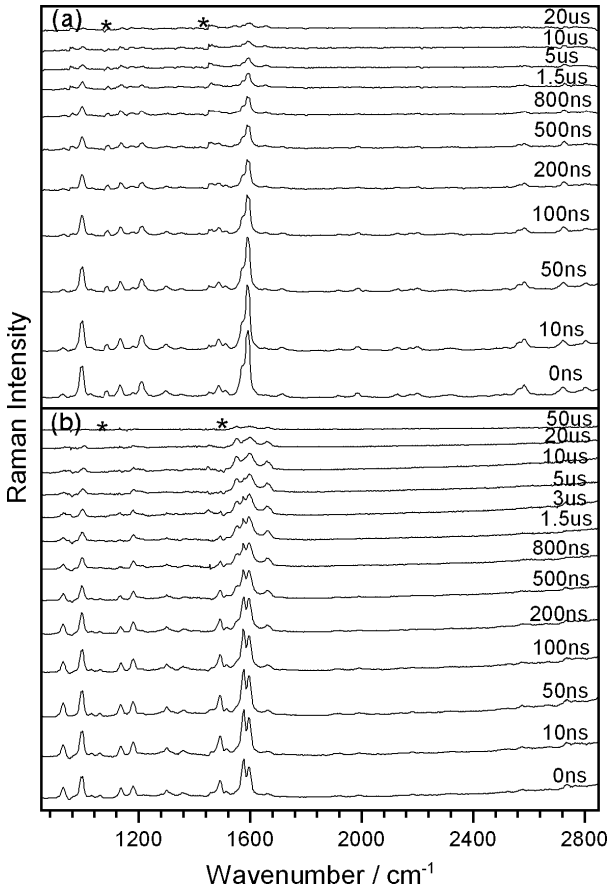

Figure 7. Nanosecond time-resolved resonance Raman of 4-BPy in 2-propanol obtained with 266 nm pump excitation wavelength and 319.9 nm (a), 354.7 nm (b) probe wavelengths at various delay times that indicated next to the spectra. The asterisk (*) mark subtraction artifacts.

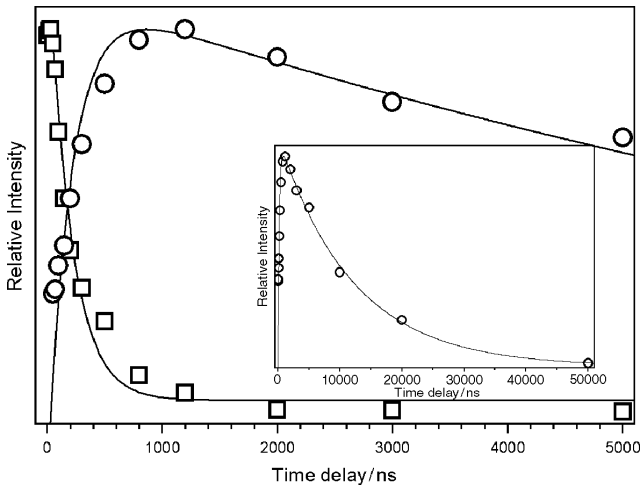

Figure 8. Time dependence of the 1575 cm^{-1} (open square decay time about 202 ns) and 1662 cm^{-1} (open circle growth time about 207 ns and decay time about 12.1 μs) band area obtained in Fig. 7(b). The inset displays the whole dynamic view of 1662 cm^{-1} at 50 μs in the experiment. Solid lines are the results of fits to the experimental data (see the text for the more details).

band that can be used to monitor the time-dependent behavior of this species (see data points in Fig. 8). A fit to this data (solid line) is displayed in Fig. 8, which shows that the new species has an exponential growth time constant of ~207 ns. The time constants for the decay of 4-BPy ketyl (~202 ns) and the growth of the new species (~207 ns) are close to each other and within the uncertainty of the measurements, and this indicates that the 4-BPy ketyl radical is a precursor for the formation of the new species. Since the 4-BPy ketyl radical TR^3 band decay corresponds to the growth of the new species TR^3 bands in the spectra of Fig. 7, it is probable that the 4-BPy ketyl radical is reacting very fast with another species to form a new species observed in the TR^3 spectra. Since the hydrogen- abstraction reaction of the triplet 4-BPy with the 2-propanol which forms the 4-BPy ketyl radical also produces a DMK radical, a cross-coupling reaction of the 4-BPy ketyl radical with the DMK radical probably takes place to a significant extent. Previous work found that the formation of the DPK radical and DMK radical would subsequently react to mainly make the *para*-LAT but not *ortha*-LAT cross-coupling product after photolysis of BP in 2-propanol.[55] Therefore, the analogous *para*-cross-coupling reactions of the 4-BPy ketyl radical with the DMK radical attack on the *para*-**N** atom position of the pyridine ring to form a cross-coupling product like 2-[4-(hydroxy-phenyl-methylene)-4H-pyridin-1-yl]-propan-2-ol and by their attack on the *para*-**C** atom position of the phenyl ring to form a cross-coupling product like 2-[4-(hydroxy-pyridin-4-yl-methyl)-cyclohexa-2,5-dienyl]-propan-2-ol were explored as likely possibilities. The B3LYP/6–311G** DFT total energy (including ZPE) calculations found that *para*-**N** atom position LAT, 2-[4-(hydroxy-phenyl-methylene)-4H-pyridin-1-yl]-propan-2-ol, is about 23.4 kJ mol^{-1} more stable than that of *para*-C atom position LAT, 2-[4-(hydroxy-pyridin-4-yl-methyl)-cyclohexa-2,5-dienyl]-propan-2-ol species. This suggests that it is more difficult for the DMK radical to react at the *para*-**C** site compared to the *para*-**N** site of the 4-BPy ketyl radical and would likely kinetically lead to production of more 2-[4-(hydroxy-phenyl-methylene)-4H-pyridin-1-yl]-propan-2-ol (which is denoted as *para*-**N**-LAT hereafter). B3LYP/6–311G** DFT calculations were performed to determine the optimized structures of the *para*-**N**-LAT cross-coupling products (see Fig. 9(b) for a schematic diagram of the optimized geometry structures).

Figure 10 displays a comparison between the experimental TR^3 spectrum obtained at 10 ns and 10 μs in Fig. 7 to the B3LYP/6–311G** DFT-calculated normal Raman spectra for the 4-BPy ketyl radical (Fig. 10(c)) and *para*-**N**-LAT (Fig. 10(e)) cross-coupling products. Inspection of Fig. 10 reveals that the calculated normal Raman spectra

DOI: 10.1002/jrs

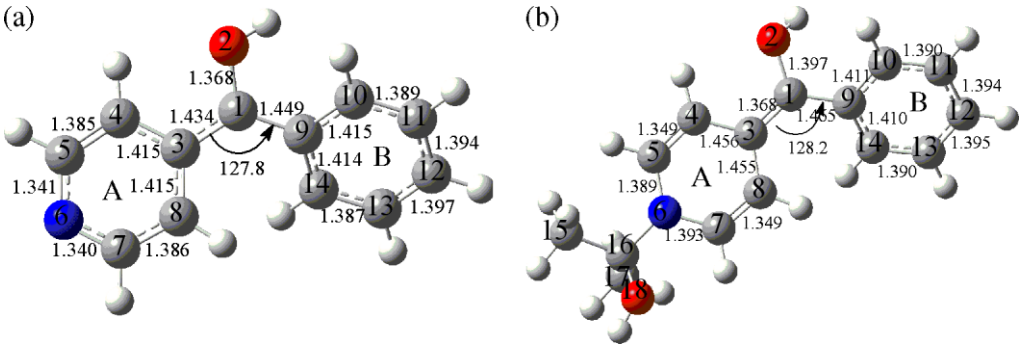

Figure 9. Optimized structure of the ketyl radical (a) and *para*-**N**-LAT of 4-BPy (b) calculated from the B3LYP/6–31G** DFT calculations. Selected bond lengths (in Å) and bond angles (in deg) are labeled. This figure is available in colour online at www.interscience.wiley.com/journal/jrs.

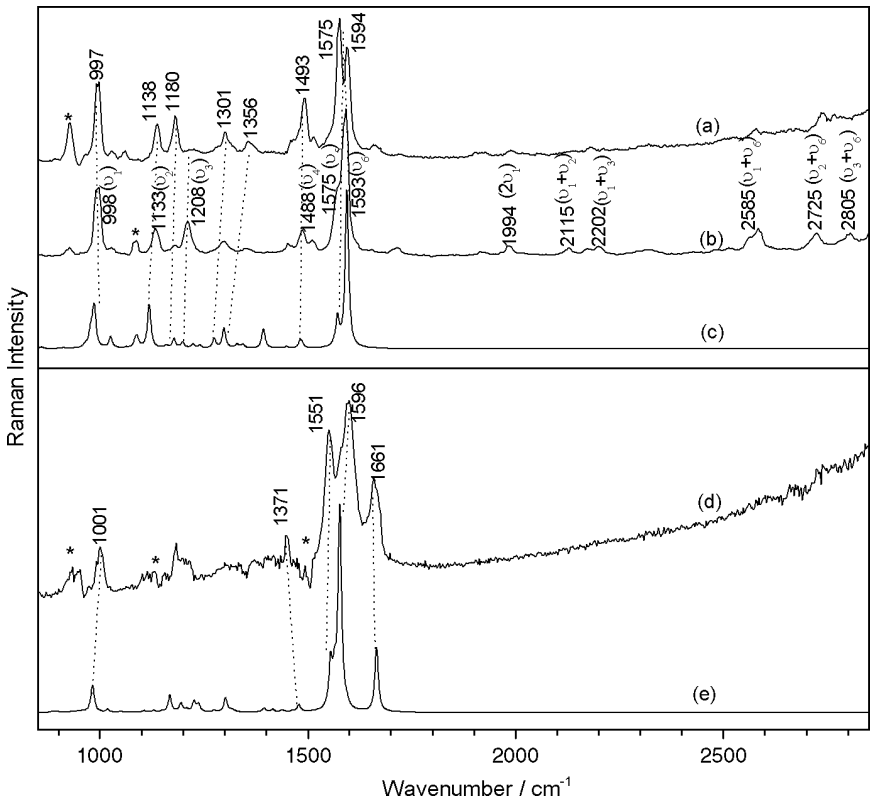

Figure 10. Comparison of the experimental resonance Raman spectra of 4-BPy obtained in 2-propanol 10 ns delay time with 354.7 nm (a) and 319.9 nm (b) probe wavelength and 10 μs delay time (d) with the DFT-calculated spectra for the 4-BPy ketyl radical (c) and *para*-**N**-LAT (e). The asterisk (*) marks subtraction artifacts. Dotted lines display the correlation between the experimental and calculated Raman bands (see text for more details).

for the 4-BPy ketyl radical (Fig. 10(c)) and the *para*-**N**-LAT cross-coupling product (Fig. 10(e)) exhibit reasonable agreement with the experimental TR[3] spectra acquired at 10 ns (Fig. 10(a) and (b)) and 10 μs (Fig. 10(d)), respectively. The experimental and calculated spectra in Fig. 10 show moderate differences in their relative Raman intensity pattern. This can be rationalized by the experimental spectra being resonantly enhanced, whereas the calculated spectra are nonresonant Raman spectra. Preliminary Raman band assignments for the *para*-**N**-LAT cross-coupling product were made on the basis of the correlation between the experimental and calculated Raman spectra displayed in Fig. 10(d) and (e). Table 3S lists the tentative vibrational assignments with nominal descriptions of the normal modes. Examination of Fig. 10 and Table 3S shows that the calculated vibrational wavenumbers for the *para*-**N**-LAT species agree well with

the experimentally observed TR^3 Raman bands. The results in Table 5S from TD-DFT (B3LYP/6–311G**) calculations indicate that at wavelengths longer than 300 nm the *para*-**N**-LAT species has only one strong electronic transition at about 368 nm with a predicted oscillator strength of 0.455. This correlates well with the long-lived *para*-**N**-LAT species observed in the TR^3 spectra of Fig. 3 having strong intensity in the 354.7 nm probe wavelength and noticeably weaker intensity for the 319.9 probe wavelength spectra. The TR^3 results here indicate that the formation of the *para*-**N**-LAT cross-coupling product from the reaction of the 4-BPy ketyl radical and the DMK radical directly correlates with the decay of the 4-BPy ketyl radical species and both take place with a time constant of about 200 ns under the conditions used in the experiments reported here.

The structure and properties of 4-BPy ketyl radical and the *para*-**N**-LAT species are different from each other. Figure 9 presents some selected bond lengths and bond angles for 4-BPy ketyl radical and the *para*-**N**-LAT species, and Table 2 gives a more comprehensive list of the structural parameters. Inspection of the structures shown in Fig. 9 reveals that when the 4-BPy ketyl radical reacts with DMK radical to produce the *para*-**N**-LAT species, the structure of the ring A part that connects with DMK radical significantly changes its structure. For example, the C1–C3, C4–C5, and C7–C8 bonds become noticeably shorter with lengths around 1.35 Å and have the typical double bond character. This indicates that the cross-coupling reaction results in the ring A having a cyclohexadienyl character with an enol moiety attached to this ring in the *para*-**N**-LAT species (Fig. 9). This increase of cyclohexadienyl character in ring A is accompanied by noticeable changes in the enol moiety, the bonds connecting ring A and ring B, and the relative orientation between the two rings. For example, the C1–C3 and C1–C9 bonds connecting the two rings go from 1.434 and 1.449 Å in the 4-BPy ketyl radical to become 1.368 and 1.465 Å, respectively, in the *para*-**N**-LAT species. This indicates that the C1–C3 bond gains double-bond character resulting in the enol formation, whereas the C1–C9 bond gains more single-bond character. These changes appear to be an extension of the cyclohexadienyl conjugation system and it is interesting to note that the ring A C4–C5 and C7–C8 bonds have somewhat stronger double-bond (bond lengths of 1.349 Å) character than the enol C1–C3 bond (1.368 Å). The bond lengths of N6–C5 and N6–C7 in ring A of *para*-**N**-LAT are significantly lengthened to about 1.390 Å compared to the about 1.340 Å length for the corresponding bonds of the 4-BPy ketyl radical. The most intense Raman bands observed for the TR^3 spectra of the *para*-**N**-LAT species that are assigned to the long-lived LAT intermediate are mainly due to vibrations associated with the C–C stretching motions of the phenyl rings and the enol moiety (Table 3S). For example, the 1661 cm^{-1} Raman mode has motions predominantly in the C–C stretching of ring A, C1–C3–C9, and O2–H bending motions; the 1596 cm^{-1} Raman mode has contributions mostly from the C–C stretching of ring B, C1–C3–C9, and O2–H bending motions; and the 1551 cm^{-1} Raman mode has contributions

Table 2. Structural parameters for the ketyl radical and *para* N-LAT of 4-BPy calculated from the DFT calculations using the B3LYP methods and a 6-311G** basis set

Bond lengths(Å)			Bond angles(deg)			Dihedral angles(deg)		
	BPy radical	BPy LAT		BPy radical	BPy LAT		BPy radical	BPy LAT
C1–O2	1.368	1.397	C1–C3–C4	120.5	121.2	C1–C3–C4–C5	−179.2	179.4
C1–C3	1.434	1.368	C1–C9–C10	119.8	119.7	C1–C9–C10–C11	−177.4	−178.1
C1–C9	1.449	1.465	C3–C1–O2	114.5	116.3	O2–C1–C3–C4	16	8.1
C3–C4	1.415	1.456	C3–C1–C9	127.8	128.2	O2–C1–C9–C10	27	29.1
C4–C5	1.385	1.349	C9–C1–O2	117.7	115.4	C3–C4–C5–N6	0.5	2.4
C5–C6	1.341	1.389	C3–C4–C5	119.5	122.1	C4–C5–N6–C7	0.7	0.3
N6–C7	1.34	1.393	C4–C5–N6	124.5	122.9	C5–N6–C7–C8	−0.8	−1
N7–C8	1.386	1.349	C5–N6–C7	116.1	116.8	N6–C7–C8–C3	−0.4	−0.9
C8–C3	1.415	1.455	N6–C7–C8	124.5	122.8	C9–C10–C11–C12	0.2	0.4
C9–C10	1.415	1.411	C7–C8–C3	119.4	122.1	C10–C11–C12–C13	0.2	0.6
C10–C11	1.389	1.39	C8–C3–C4	116	113.1	C11–C12–C13–C14	−0.1	−0.3
C11–C12	1.394	1.394	C9–C10–C11	121.1	121.2	C12–C13–C14–C9	−0.3	−0.9
C12–C13	1.397	1.395	C10–C11–C12	120.4	120.5			
C13–C14	1.387	1.39	C11–C12–C13	119.3	119.1			
C14–C9	1.414	1.41	C12–C13–C14	120.7	120.6			
C15–C16		1.533	C13–C14–C9	120.8	121.1			
C16–N6		1.474						
C16–C17		1.537						
C16–O18		1.431						

DOI: 10.1002/jrs

mostly from the C–C stretching of ring A and B, C1–C3–C9, and O2–H bending motions. The vibrational mode mostly due to C–C stretching of ring A in the *para*-**N**-LAT species is at 1661 cm^{-1} which displays an upshift of about 86 cm^{-1} compared to the corresponding mode width of the 4-BPy ketyl radical which is at 1575 cm^{-1}. This is also in good agreement with the DFT structural results, which show that the ring A C4–C5 and C7–C8 bonds have stronger double-bond character than those in ring A of the 4-BPy ketyl radical.

Some previous studies[8,13] observed that the decay of the LAT intermediate with an absorption maximum at about 358 nm formed from photolysis of BP in 2-propanol depends on the concentration of BP. This indicates that the LAT intermediate is likely reacting with the parent BP to produce the final products (e.g. a reaction like *para*-DPK-DMK + BP → benzopinacol + acetone is a possibility) observed in photochemistry experiments. We think a similar process would transform the similar LAT cross-coupling product observed here for the closely related 4-BPy system into the analogous final products observed in photochemistry experiments. Further work to more explicitly characterize the decay of the LAT species and the formation of its decay products would be an attractive topic for future study.

To summarize, we propose the following as the main reaction pathways for the 266 nm photoexcitation of 4-BPy in neat MeCN and 2-propanol solvents on the basis of our present TR^3 study (see in Scheme 2). In neat MeCN, only the photophysical associated processes including photoexcitation, efficient ISC from the singlet to triplet, and relaxation of the excess energy to come back the parent ground state (after about 176 ns for the reaction conditions reported here) appear to occur to an appreciable extent. In 2-propanol solvent, the reactivity of the $n\pi^*$ triplet 4-BPy is very high for the hydrogen-abstraction reaction with the 2-propanol solvent molecules so that this reaction is very fast so that no signal from the triplet 4-BPy was observed in the early time delay spectra (such as at 10 ns) in contrast to observation of the BP triplet under similar reaction conditions in 2-propanol solvent.[55] This implies that the triplet 4-BPy species is more reactive than the triplet BP species for hydrogen abstraction of 2-propanol. The 4-BPy ketyl radical species is produced from the hydrogen-abstraction reaction of the triplet 4-BPy with 2-propanol and decays with a time constant of about 200 ns time owing to recombination of 4-BPy ketyl radical and an associated DMK radical (from the hydrogen-abstraction reaction with the solvent) to form the *para*-**N**-LAT intermediate.

CONCLUSION

A ns-TR^3 spectroscopic investigation of the triplet state 4-BPy reaction with 2-propanol (a good hydrogen-donor solvent) and subsequent reactions was described. The TR^3 spectra observed the 4-BPy triplet state ($n\pi^*$) hydrogen-abstraction reaction with 2-propanol took place in less than 10 ns time scale to produce a 4-BPy ketyl radical and an associated dimethyl ketyl radical, and recombination of these two radical species via a cross-coupling reaction took place with a time constant of about 200 ns to produce a *para*-**N**-LAT intermediate under the reaction conditions employed in our study. The comparison of the TR^3 spectra to results from DFT calculations were used to identify these intermediates. The structure and properties of the 4-BPy triplet, 4-BPy ketyl radical, and *para*-**N**-LAT species were discussed. The electron-withdrawing effect of the heterocyclic nitrogen for 4-BPy on the triplet state gives it a significantly higher chemical reactivity for the hydrogen abstraction with 2-propanol compared to the corresponding BP triplet reaction under similar reaction conditions. In addition, the 4-BPy ketyl radical reacts with the dimethyl ketyl radical to attach at the *para*-N atom position of the pyridine ring to form a cross-coupling product like 2-[4-(hydroxy-phenyl-methylene)-4H-pyridin-1-yl]-propan-2-ol instead of attacking at the *para*-C atom position as was observed for the corresponding BP reaction LAT cross-coupling product reported in an earlier study.

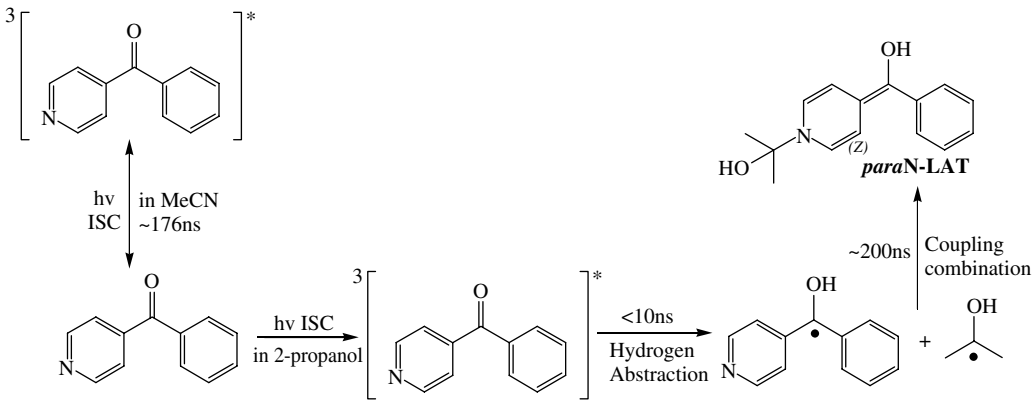

Scheme 2. Proposed reaction pathways for the photolysis of 4-benzoylpyridine in pure MeCN and 2-propanol solvents. See text for details.

DOI: 10.1002/jrs

Supplementary material

Supplementary electronic material for this paper is available in Wiley InterScience at: http://www.interscience.wiley.com/jpages/0377-0486/suppmat/

Acknowledgements

This research has been supported by grants from the Research Grants Council of Hong Kong (HKU7040/06P), the award of a Croucher Foundation Senior Research Fellowship (2006–2007) from the Croucher Foundation, and an Outstanding Researcher Award (2006) from the University of Hong Kong to DLP. WMK thanks the University of Hong Kong for the award of a Research Assistant Professor position.

REFERENCES

1. Turro NJ. *Modern Molecular Photochemistry*. University Science Books: Mill Valley, 1991.
2. Moore WM, Hammond GS, Foss RP. *J. Am. Chem. Soc.* 1961; **83**: 2789.
3. El-Sayed MA. *J. Chem. Phys.* 1963; **38**: 2834.
4. Godfrey TS, Hilpern JW, Porter G. *Chem. Phys. Lett.* 1967; **1**: 490.
5. Rentzepis PM. *Science* 1970; **169**: 239.
6. Hochstrasser RM, Wessel JE. *Chem. Phys. Lett.* 1973; **19**: 156.
7. Anderson RW Jr, Hochstrasser RM, Lutz H, Scott GW. *J. Chem. Phys.* 1974; **61**: 2500.
8. Hochstrasser RM, Lutz H, Scott GW. *Chem. Phys. Lett.* 1974; **24**: 162.
9. Hochstrasser RM, Lutz H, Scott GW. *Chem. Phys. Lett.* 1974; **28**: 153.
10. Topp MR. *Chem. Phys. Lett.* 1975; **32**: 144.
11. Bensasson RV. *J. Chem. Soc., Faraday I* 1980; **76**: 1801.
12. Peters KS, Freilich SC, Schaeffer CG. *J. Am. Chem. Soc.* 1980; **102**: 5701.
13. Wagner PJ, Truman RJ, Scaiano JC. *J. Am. Chem. Soc.* 1985; **107**: 7093.
14. Ohzeki T, Ohgus H, Isaka H, Suzuki S, Takahashi T. *Chem. Phys. Lett.* 1988; **149**: 379.
15. McGarry PF, Doubleday CE Jr, Wu C, Staab HA, Turro NJ. *J. Photochem. Photobiol., A* 1994; **77**: 109.
16. Bhasikuttan AC, Singh AK, Palit DK, Sapre AV, Mittal JP. *J. Phys. Chem. A* 1998; **102**: 3470.
17. Prater K, Freund WL, Bowman RM. *Chem. Phys. Lett.* 1998; **295**: 82.
18. Cai X, Sakamoto M, Hara M, Sugimoto A, Tojo S, Kawai K, Endo M, Fujitsuka M, Majita T. *Photochem. Photobiol. Sci.* 2003; **2**: 1209.
19. Okustu T, Muramatsu H, Horiuchi H, Hiratsuka H. *Chem. Phys. Lett.* 2005; **404**: 300.
20. Miyasaka H, Morita K, Kamada K, Mataga N. *Bull. Chem. Soc. Jpn.* 1990; **63**: 131.
21. Tamai N, Asahi T, Masuhara H. *Chem. Phys. Lett.* 1992; **198**: 413.
22. Ramseier M, Senn P, Wirz J. *J. Phys. Chem. A* 2003; **107**: 3305.
23. Shah BK, Neckers DC. *J. Am. Chem. Soc.* 2004; **126**: 1830.
24. Shah BK, Rodgers MAJ, Neckers DC. *J. Phys. Chem. A* 2004; **108**: 6087.
25. Sakamoto M, Cai X, Hara M, Tojo S, Fujitsuka M, Majita T. *J. Phys. Chem. A* 2004; **108**: 8147.
26. Cai X, Sakamoto M, Fujitsuka M, Majima T. *Chem. Eur. J.* 2005; **11**: 6471.
27. Sakamoto M, Cai X, Fujitsuka M, Majima T. *Chem. Eur. J.* 2006; **12**: 1610.
28. Pitts JN Jr, Letsinger RL, Taylor RP, Patterson JM, Recktenwald G, Martin RB. *J. Am. Chem. Soc.* 1959; **81**: 1068.
29. Beckett A, Porter G. *Trans. Faraday Soc.* 1963; **59**: 2038.
30. Backström HLJ, Appelgren KL, Niklasson RJV. *Acta Chem. Scand.* 1965; **19**: 1555.
31. Schenck GO, Cziesla M, Eppinger K, Matthias G, Pape M. *Tetrahedron Lett.* 1967; **3**: 193.
32. Filipescu N, Minn FL. *J. Am. Chem. Soc.* 1968; **90**: 1544.
33. Chilton J, Guering L, Steel C. *J. Am. Chem. Soc.* 1976; **98**: 1865.
34. Colman P, Dunne A, Quinn MF. *J. Chem. Soc., Faraday Trans. I* 1976; **72**: 2605.
35. Rubin MB. *Tetrahedron Lett.* 1982; **23**: 4615.
36. Demeter A, László B, Bérces T. *Ber. Bunsenges. Phys. Chem.* 1988; **92**: 1478.
37. Demeter A, Bérces T. *J. Photochem. Photobiol., A: Chem.* 1989; **46**: 27.
38. Demeter A, Bérces T. *J. Phys. Chem.* 1991; **95**: 1228.
39. Albini A, Bortolus P, Fasini E, Monti S, Negri F, Orlandi G. *J. Chem. Soc., Perkin Trans.* 1993; **2**: 691.
40. Viltres Costa C, Grela MA, Churio MS. *J. Photochem. Photobiol., A: Chem.* 1996; **99**: 51.
41. Fister JC, Harris JM. *Anal. Chem.* 1995; **67**: 701.
42. Tahara T, Hamaguchi H, Tasumi M. *J. Phys. Chem.* 1987; **91**: 5875.
43. Tahara T, Hamaguchi H, Tasumi M. *Chem. Phys. Lett.* 1988; **152**: 135.
44. Tahara T, Hamaguchi H, Tasumi M. *J. Phys. Chem.* 1990; **94**: 170.
45. Yabumoto S, Sato S, Hamaguchi H. *Chem. Phys. Lett.* 2005; **416**: 100.
46. Bosca F, Miranda MA. *J. Photochem. Photobiol., B* 1998; **43**: 1.
47. Ortica F, Elisei F, Favaro G. *J. Phy. Org. Chem.* 1999; **12**: 31.
48. Bortolus P, Elisei F, Favaro G, Monti S, Ortica F. *J. Chem. Soc., Faraday Trans.* 1996; **92**: 1841.
49. Ortica F, Elisei F, Favaro G. *J. Chem. Soc., Faraday Trans.* 1995; **91**: 3405.
50. Ortica F, Favaro G, Elisei F. *J. Chem. Soc., Faraday Trans.* 1994; **90**: 279.
51. Favaro G, Masetti F, Romani A. *J. Photochem. Photobiol., A* 1990; **53**: 41.
52. Elisei F, Favaro G, Romani A. *Chem. Phys.* 1990; **144**: 107.
53. Favaro G. *J. Photochem.* 1980; **15**: 89.
54. Favaro G. *J. Photochem.* 1986; **33**: 261.
55. Du Y, Ma C, Kwok WM, Xue J, Phillips DL. *J. Org. Chem.* 2007; **72**: 7148.
56. Anandhi R, Umapathy S. *J. Raman Spectrosc.* 2000; **31**: 331.
57. Zhu P, Ong SY, Chan PY, Leung KH, Phillips DL. *J. Am. Chem. Soc.* 2001; **123**: 2645.
58. Li YL, Leung KH, Phillips DL. *J. Phys. Chem. A* 2001; **105**: 10621.
59. Zhu P, Ong SY, Chan PY, Poon YF, Leung KH, Phillips DL. *Chem. Eur. J.* 2001; **7**: 4928.
60. Chan PY, Ong SY, Zhu P, Leung KH, Phillips DL. *J. Org. Chem.* 2003; **68**: 5265.
61. Chan PY, Ong SY, Zhu P, Zhao C, Phillips DL. *J. Phys. Chem. A* 2003; **107**: 8067.
62. Chan PY, Kwok WM, Lam SK, Chiu P, Phillips DL. *J. Am. Chem. Soc.* 2005; **127**: 8246.
63. Xue J, Guo Z, Chan PY, Chu LM, But TYS, Phillips DL. *J. Phys. Chem. A* 2007; **111**: 1441.
64. Frisch MJ, Trucks GW, Schlegel HB, Scuseria GE, Robb MA, Cheeseman JR, Zakrzewski VG, Montgomery JA Jr, Stratmann RE, Burant JC, Dapprich S, Millam JM, Daniels AD, Kudin KN, Strain MC, Farkas O, Tomasi J, Barone V, Cossi M, Cammi R, Mennucci B, Pomelli C, Adamo C, Clifford S, Ochterski J, Petersson GA, Ayala PY, Cui Q, Morokuma K, Malick DK, Rabuck AD, Raghavachari K, Foresman JB, Cioslowski J, Ortiz JV, Baboul AG, Stefanov BB, Liu G, Liashenko A, Piskorz P, Komaromi I, Gomperts R Martin RL, Fox DJ, Keith T, Al-Laham MA, Peng CY, Nanayakkara A, Gonzalez C, Challacombe M, Gill PMW, Johnson B, Chen W, Wong MW,

Andres JL, Gonzalez C, Head-Gordon M, Replogle ES, Pople JA. *Gaussian 98 revision A.7*. Gaussian: Pittsburgh, 1998.
65. Frisch MJ, Trucks GW, Schlegel HB, Scuseria GE, Robb MA, Cheeseman JR, Zakrzewski VG, Montgomery JA Jr, Stratmann RE, Burant JC, Dapprich S, Millam JM, Daniels AD, Kudin KN, Strain MC, Farkas O, Tomasi J, Barone V, Cossi M, Cammi R, Mennucci B, Pomelli C, Adamo C, Clifford S, Ochterski J, Petersson GA, Ayala PY, Cui Q, Morokuma K, Malick DK, Rabuck AD, Raghavachari K, Foresman JB, Cioslowski J, Ortiz JV, Baboul AG, Stefanov BB, Liu G, Liashenko A, Piskorz P, Komaromi I, Gomperts R Martin RL, Fox DJ, Keith T, Al-Laham MA, Peng CY, Nanayakkara A, Gonzalez C, Challacombe M, Gill PMW, Johnson B, Chen W, Wong MW, Andres JL, Gonzalez C, Head-Gordon M, Replogle ES, Pople JA *Gaussian 03 revision B.05*. Gaussian: Pittsburgh, 2003.
66. Balakrishnan G, Umapathy S. *Chem. Phys. Lett.* 1997; **270**: 557.
67. Balakrishnan G, Mohandas P, Umapathy S. *J. Phys. Chem. A* 2001; **105**: 7778.
68. Biswas N, Umapathy S. *Chem. Phys. Lett.* 1998; **294**: 181.
69. Puranik M, Umapathy S, Snijders JG, Chandrasekhar J. *J. Chem. Phys.* 2001; **115**: 6106.

DOI: 10.1002/jrs